Nuclear Inst. and Methods in Physics Research, A 956 (2020) 163331

Contents lists available at ScienceDirect

Nuclear Inst. and Methods in Physics Research, A

journal homepage: www.elsevier.com/locate/nima

Performance of the GridPix detector quad

C. Ligtenberg [a,*], Y. Bilevych [b], K. Desch [b], H. van der Graaf [a], M. Gruber [b], F. Hartjes [a], K. Heijhoff [a,b], J. Kaminski [b], P.M. Kluit [a], N. van der Kolk [a], G. Raven [a], T. Schiffer [b], J. Timmermans [a]

[a] Nikhef, Science Park 105, 1098 XG Amsterdam, The Netherlands
[b] Physikalisches Institut, University of Bonn, Nussallee 12, 53115 Bonn, Germany

ARTICLE INFO

Keywords:
Micromegas
Gaseous pixel detector
Micro-pattern gaseous detector
Timepix
GridPix
Time projection chamber

ABSTRACT

A gaseous pixel readout module with four GridPix chips, called the quad, has been developed as a building block for a large time projection chamber readout plane. The quad module has dimensions 39.6 mm × 28.38 mm and an active surface coverage of 68.9%. The GridPix chip consists of a Timepix3 chip with integrated amplification grid and have a high efficiency to detect single ionization electrons, which enable to make a precise track position measurement. A quad module was installed in a small time projection chamber and measurements of 2.5 GeV electrons were performed at the ELSA accelerator in Bonn, where a silicon telescope was used to provide a reference track. The error on the track position measurement, both in the pixel plane and drift direction, is dominated by diffusion. The quad was designed to have minimum electrical field inhomogeneities and distortions, achieving systematics of better than 13 μm in the pixel plane. The resolution of the setup is 41 μm, where the total systematic error of the quad detector is 24 μm.

1. Introduction

In drift chambers charged particles are identified through ionization in the gas. For the readout of a time projection chamber (TPC) the finest granularity is offered by pixel readouts. In particular, a GridPix is a CMOS pixel readout chip with an integrated amplification grid added by MEMS postprocessing techniques [1,2]. As a result, single ionization electrons can be detected with great precision, allowing an excellent track position measurement and an estimate of the number of clusters for an energy loss (dE/dx) measurement for particle identification.

The original GridPix using the Timepix chip [3] has recently been succeeded by a GridPix based on the Timepix3 chip [4]. This newer chip offers superior timing, faster readout speed and the possibility to apply time walk corrections. The first results of a single chip detector have been analyzed and published in [5]. Electron diffusion in gas was found to be the dominant error on the track position measurement and systematics in the pixel plane remained below 10 μm. Using a truncated sum, an energy loss (dE/dx) resolution of 4.1 % was found for an effective track length of 1 m. The single chip detector was operated reliably in a test beam experiment. However, equipping a large detector surface poses an entirely new challenge.

In order to cover a large detector surface, it is practical to subdivide it into a number of standardized modules. Here we present the design of a quad module with four Timepix3 chips. Because the quad module has all services under the active area, it can be tiled to cover arbitrarily large areas. The performance of a TPC, read out by a single quad module was tested at the ELSA test beam facility in Bonn. Possible applications are in TPCs at future electron–positron colliders, other particle physics experiments and medical imaging such as proton therapy [3,6].

2. Quad detector design and construction

2.1. The Timepix3 based GridPix

Here the GridPix consists of a Timepix3 chip with an integrated grid. Directly on the surface of the Timepix3 chip, a 4 μm thick silicon-rich silicon nitride protection layer is deposited in order to prevent damage of the readout chip from discharges. On top of this 50 μm high SU8 pillars are attached that support the 1 μm thick aluminum grid that has 35 μm diameter circular holes aligned to the pixel input pads. The grid and dykes design was reoptimized: at four sides the grid ends on a solid SU8 dyke for which on two sides three readout columns were given up. The Timepix3 chip has a low equivalent noise charge (≈70 e^-) and allows for a simultaneous measurement of the Time of Arrival (ToA) and the Time over Threshold (ToT) using a TDC (clock frequency 640 MHz) per pixel. For the readout, one out of the eight available links per chip is connected to a speedy pixel detector readout (SPIDR) board [7] at a speed of 80 Mbps. The hardware allows reading out at twice this speed.

* Corresponding author.
E-mail address: cligtenb@nikhef.nl (C. Ligtenberg).

https://doi.org/10.1016/j.nima.2019.163331
Received 8 October 2019; Received in revised form 18 December 2019; Accepted 22 December 2019
Available online 24 December 2019

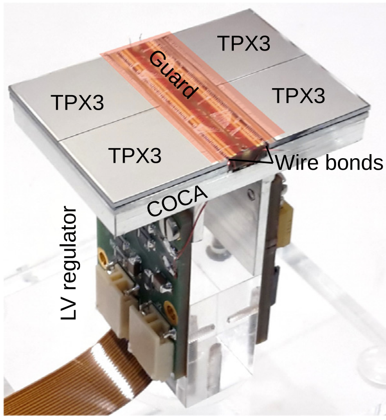

Fig. 1. Picture of the quad detector with four Timepix3 GridPixes (TPX3) mounted on a cold carrier plate (COCA). The central guard was omitted to show the wire bond PCB, and its operating position is indicated with a transparent rectangle. On the left the Low Voltage (LV) regulator and flexible Kapton cable are visible.

2.2. The quad module design and assembly

In order to cover large areas, the quad module shown in Fig. 1 was developed. Because of the complexity of the GridPix technology and the fragility of the grids, a small number of four chips per module was chosen. The chips are mounted on a common cooled base plate (COCA). They are electrically connected by wire bonds to a 6 mm wide PCB between the two pairs of chips. This allows the control and output lines to be directed to the backside of the quad to maximize the sensitive detection area. A short Kapton cable at the other side of the wire bond PCB provides a low impedance connection to the low voltage (LV) regulator. The grids are connected by 80 μm insulated copper wires to a high voltage (HV) filtering board. The connection to the common HV input uses a 100 MΩ resistor for each grid to rapidly quench a micro-discharge. To support and cool the LV regulator board and the HV filtering board, a U-shaped support is attached by thermally conductive glue under the carrier plate. Finally, the wire bonds of the quad are covered by a 10 mm wide central guard electrode located 1.1 mm above the grids to maintain a homogeneous drift field.

The external quad dimensions are 39.6 mm × 28.38 mm of which 68.9% is active. In the present design the support components are made of aluminum contributing substantially to the material budget. In the future the material budget can be further minimized by replacing the aluminum by carbon based materials. During low rate operation, the module consumes 8 W of power of which 2 W in the LV regulator.

2.3. The quad detector

The quad module was embedded in a TPC consisting of a steel box and a 40 mm high field cage to provide a homogeneous drift field. The sides of the field cage are formed by 75 μm CuBe wires with a 2 mm pitch to facilitate UV laser beam measurements. The field cage is terminated on one end by the quad module fitted in a closely surrounding coppered frame at the grid potential, and on the other end by a solid cathode plate. The whole structure was put in a gas-tight container with 50 μm Kapton windows on two sides to minimize the material traversed by the beam.

3. Test beam measurement

The device was tested in October 2018 at the ELSA test beam facility in Bonn. The ELSA accelerator provided 2.5 GeV electrons at a rate of approximately 10 kHz during spills of 16.0 s in beam cycles of 17.1 s. The whole quad detector was mounted on a remotely controlled slider stage. To provide a precise reference track, the quad TPC was sandwiched between 2 × 3 planes of a Mimosa26 telescope [8], see Fig. 2. Each plane consists of a MAPS detector with 1152 × 576 pixels of size 18.4 μm × 18.4 μm.

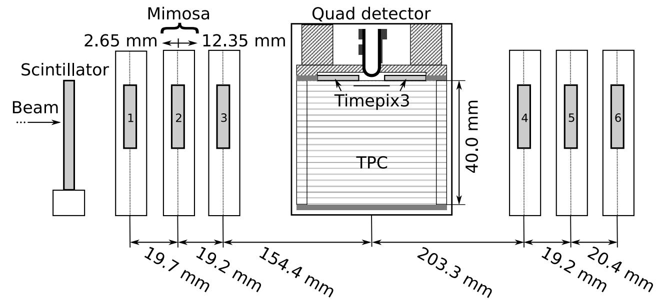

Fig. 2. Setup of the quad with telescope at the ELSA test beam facility.

Table 1
Parameters of the three analyzed runs. The error on the temperature and pressure indicates the spread in the time the three runs were taken.

Runs duration	10 min
Triggers per run	2.2×10^6 triggers
V_{grid}	330 V
E_{drift}	400 V/cm
Threshold	550 e^-
Temperature	(300.5 ± 0.13) K
Pressure	(1011 ± 0.16) mbar
Oxygen concentration	814 ppm
Water vapor concentration	6000 ppm

A scintillator provided a trigger signal to the Trigger Logic Unit (TLU) [9] which numbers the triggers and subsequently directs them to both the SPIDR and telescope readout. The telescope hits were collected in time frames of 115.2 μs. Due to the high beam intensity, the telescope frames often contain hits from more than one track. The Timepix3 was operated in data driven mode with the trigger data merged in.

Because of the chosen limited link speed between the Timepix3 chips and the SPIDR a maximum of 1.3 MHits/s could be read out. This caused some hits to arrive late at the SPIDR readout, acquiring a wrong 409.6 μs course timestamp. As a work-around hits, up to 200 timestamps of 409.6 μm after the trigger were collected and analyzed. The first track hit had to arrive no more than 5 timestamps late, and the average course timestamp should not deviate more than 150 timestamps.

During data taking the 700 ml gas volume was flushed at a rate of 16.7 ml/min with premixed T2K TPC gas. This gas is a mixture consisting of 95 % Ar, 3 % CF_4, and 2 % iC_4H_{10} suitable for large TPCs because of the relatively high drift velocity and the low diffusion in a magnetic field. The temperature and pressure were relatively stable at 300.5 K and 1011 mbar. The gas mixture contained a 814 ppm O_2 contamination and a 6000 ppm H_2O contamination, primarily due to the high gas permeability of a silicon rubber cable feed-through.

The cathode and guard voltages were set such that the electric field was 400 V/cm, which is close to the maximum drift velocity for the contaminated gas. The grid voltage was set to 330 V, at which there is limited secondary emission from the grid by UV photons produced in avalanches. The threshold level being a trade off between noise, sensitivity and time walk, was set to about 550 e^-. The gain depends on the beam rate, because of charging up of the protection layer. During the high beam rate, the effective gain was approximately 1000. Some of the relevant run parameters are summarized in Table 1.

4. Track reconstruction and event selection

4.1. Track reconstruction procedure

Tracks are reconstructed as straight lines. The y-axis is defined roughly in the direction of the beam, and the x-axis and z-axis are in

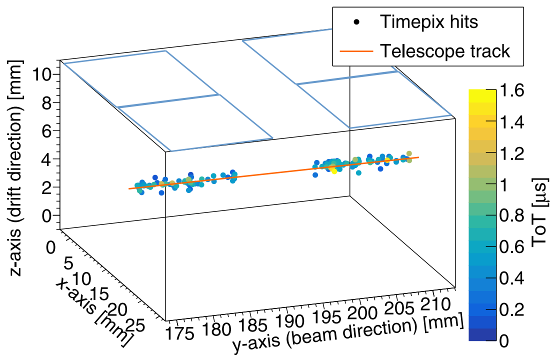

Fig. 3. An event with 148 quad detector hits and the corresponding telescope track. The positions of the chips are outlined in blue. (For interpretation of the references to color in this figure legend, the reader is referred to the web version of this article.)

the horizontal and vertical direction respectively. For the telescope, the y-coordinate is taken from the plane position, and the x-coordinate and z-coordinate correspond to the columns and rows. Apart from a small rotation, the x and y-coordinates correspond to the columns and rows of the GridPixes. The z-coordinate is the drift length calculated from the ToA and the drift velocity. Tracks are fitted using a linear regression fit with hit errors in the two directions perpendicular to the beam σ_x and σ_z. The expressions for the error values are given in Sections 5.4 and 5.5.

The detectors are aligned using the data. First, the telescope is independently aligned. The positions in the y-direction along the beam are measured and kept fixed. Taking one plane as a reference, the other five planes can be rotated. These rotations and additionally two shifts in x-direction and z-direction for four of the planes are iteratively determined from the fitted tracks. Next, the quad detector is aligned. Using iterative alignment each chip has three rotations and two shifts in the x and z-directions. Additionally, each chip has one parameter describing the angle in the xz-plane between the drift direction and the pixel plane.

An example event with a telescope track is shown in Fig. 3.

4.2. Selections

In the telescope a stringent selection is made to acquire a sample of clean tracks. At least 5 planes should have a hit and the hits should be within $50\,\mu\text{m}$ from the track. By requiring the slope difference of the track in the first three planes and in the last three planes to be smaller than 1 mrad, scattered tracks are rejected.

GridPix hits are considered if their ToA is within 500 ns of a trigger and their ToT is at least $0.15\,\mu\text{s}$. The hits are collected using a track detected by the telescope as a seed. Outliers are rejected by requiring the residuals r (pulls r/σ) with respect to the telescope track to be smaller than 1.5 mm (2.0) in the x-direction and 2.0 mm (3.0) in the z-direction.

A track is rejected if it has less than 20 hits. Moreover the average position of all Gridpix hits must be within 0.3 mm in the x-direction and z-direction of the telescope track. Given the high beam rate, the TPC often contains multiple tracks overlapping in time. To suppress overlapping tracks and to reject tracks with delta electrons, 80 % of the hits within 5 mm of a track are required to lie within a distance of 1.5 mm.

The selections are summarized in Table 2 and the total efficiency for events is about 12%. Most events are rejected, because there are less than 20 GridPix hits corresponding to the telescope track.

Table 2
Table with selection cuts.

Telescope
Number of planes hits ≥ 5
Reject outliers ($r_{x,z} < 50\,\mu\text{m}$)
Slope difference between sets of planes $<$ 1 mrad
GridPix hit selection
$-500\,\text{ns} < t_{\text{hit}} - t_{\text{trigger}} < 500\,\text{ns}$
Hit ToT $> 0.15\,\mu\text{s}$
Reject outliers ($r_x < 1.5\,\text{mm}, r_z < 2\,\text{mm}$)
Reject outliers ($r_x < 2\sigma_x, r_z < 3\sigma_z$)
Event Selection
$N_{\text{hits}} \geq 20$
$(N_{r_x<1.5\text{mm}}/N_{r_x<5\text{mm}}) > 0.8$
$\lvert x_{\text{Timepix}} - x_{\text{telescope}}\rvert < 0.3\,\text{mm}$
$\lvert z_{\text{Timepix}} - z_{\text{telescope}}\rvert < 0.3\,\text{mm}$

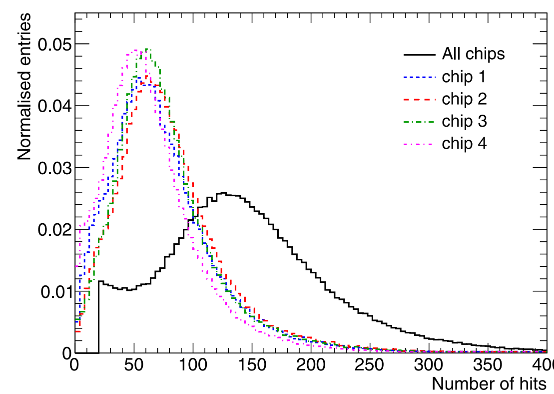

Fig. 4. Distribution of the number of hits after track selection in total and per chip.

5. Results

5.1. Number of hits

The distribution of the number of track hits per chip and the total number of track hits are shown in Fig. 4. The most probable number of hits per chip varies between 52 and 65 hits, and the mean varies between 65 and 80 hits. The most probable number of hits per quad is 131 and the mean number of track hits is 146 for an effective track length of approximately 27.5 mm. This is significantly below the calculated most probable value of 225 electron–ion pairs for a 2.5 GeV electron with this track length [10]. This is due to the too low effective grid voltage and possibly due to readout problems. Because of the low single electron efficiency, no energy loss (dE/dx) results were extracted.

5.2. Hit time corrections

To increase precision in the drift direction, the hit times were corrected. To correct for the double column structure and power distribution deformations of the Timepix3 chip, a ToT factor per column was extracted by injecting test pulses for each pixel. Furthermore, a ToA correction offset was determined from the test beam data based on the underlying substructure of 16×2 pixels due to the clock distribution. In addition one ToA correction offset per column and one offset per row was applied. The ToT corrections are of $\mathcal{O}(10\%)$ and the ToA corrections are of $\mathcal{O}(1\,\text{ns})$.

5.3. Time walk correction

A hit is registered when the collected charge reaches the threshold. Since it takes longer for a small signal to reach the threshold than it does for a large signal, the measured ToA depends on the magnitude

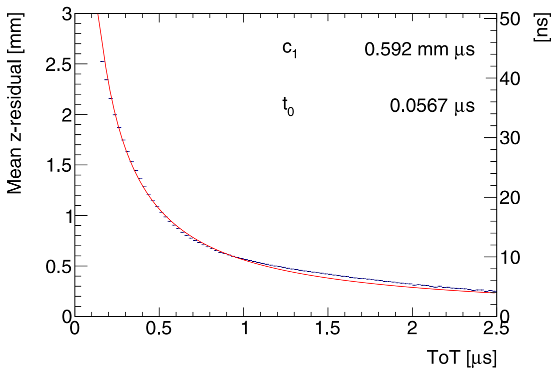

Fig. 5. Mean z-residual without time walk correction as function of ToT, fitted with Eq. (1). The right axis is given in units of ns using a drift velocity of 59 µm/ns.

of the signal. This effect is called time walk and can be corrected by using the ToT as a measure of signal magnitude. In Fig. 5 the mean of z-residuals is shown as a function of the ToT for all four chips. The relation can be parametrized using the time walk δz_{tw} as a function of the ToT t_{ToT}:

$$\delta z_{\mathrm{tw}} = \frac{c_1}{t_{\mathrm{ToT}} + t_0}, \tag{1}$$

where c_1 and t_0 are constants determined from a fit per chip.

5.4. Hit resolution in the pixel plane

The resolution of the single electrons in the transverse plane (xy) was measured as a function of the predicted drift position (z). Fig. 6 displays this relation for tracks crossing a fiducial region in the center of the chip. The resolution for the detection of ionization electrons σ_x is given by:

$$\sigma_x^2 = \frac{d_{\mathrm{pixel}}^2}{12} + D_T^2(z - z_0), \tag{2}$$

where d_{pixel} is the pixel pitch size, z_0 is the position of the grid, and D_T is the transverse diffusion coefficient. The resolution at zero drift distance $d_{\mathrm{pixel}}/\sqrt{12}$ was fixed to 15.9 µm. Tracks with a z-position around 0.3 mm are given a larger error because they scatter on the central guard. Fitting expression (2) to the data gives a transverse diffusion coefficient D_T of 398 µm/$\sqrt{\mathrm{cm}}$ with negligible statistical uncertainty. The measured value is larger than the value of 270 µm/$\sqrt{\mathrm{cm}}$ ± 3% predicted by the gas simulation software Magboltz [11]. Probably this is due to an inaccuracy in the gas mixing, which caused the CF_4 content to be lower than intended.

To compare the precision of the GridPix readout with the precision of conventional pad based TPC readouts, the resolution can be calculated over the length of one pad row. For example, at a drift distance of 4 mm the resolution of a single ionization electron is approximately 250 µm, so the resolution of a 6 mm track segment which has on average 32 electrons is therefore about 44 µm.

5.5. Hit resolution in the drift direction

The measured z-position is directly related to the drift velocity. Using the predicted positions from the telescope, the drift velocity is measured to be 54.6 µm/ns, which is slightly lower than the value of 59.0 µm/ns expected by Magboltz. Both values have negligible statistical uncertainties.

The resolution for the detection of ionization electrons σ_z is given by:

$$\sigma_z^2 = \sigma_{z0}^2 + D_L^2(z - z_0), \tag{3}$$

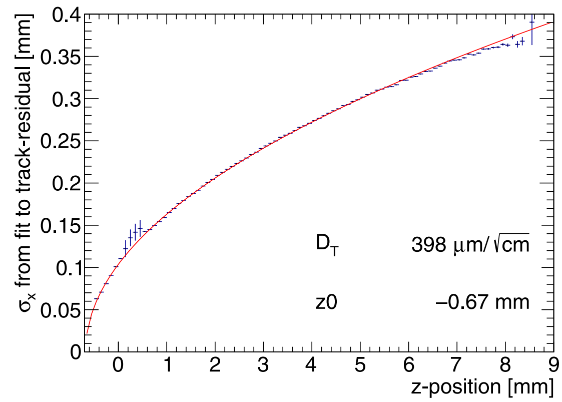

Fig. 6. Measured hit resolution in the pixel plane (blue points) fitted with the resolution function according to Eq. (2) (red line). (For interpretation of the references to color in this figure legend, the reader is referred to the web version of this article.)

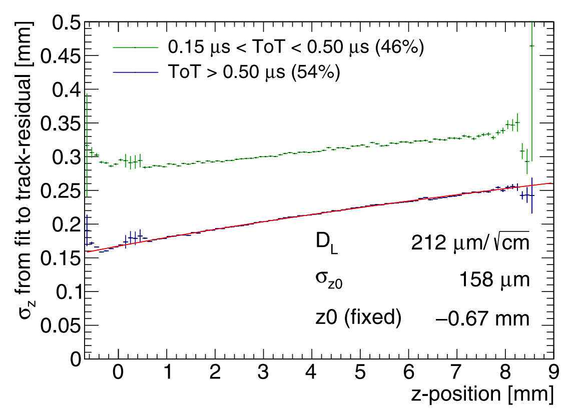

Fig. 7. Measured hit resolution in drift direction split by ToT. The hits with a ToT above 0.50 µs (blue points) are fitted with the resolution according to Eq. (3) (red line). In the legend the fractions of hits in both selections are given. (For interpretation of the references to color in this figure legend, the reader is referred to the web version of this article.)

where σ_{z0} is the resolution at zero drift distance. The resolution as function of the drift distance is shown in Fig. 7 for tracks crossing the fiducial region. Since tracks with a z-position around 0.3 mm scatter on the central guard, these data points are given a larger error. The longitudinal diffusion coefficient D_L was determined to be 212 µm/$\sqrt{\mathrm{cm}}$ with negligible statistical uncertainty, which is equal to the expected value 212 µm/$\sqrt{\mathrm{cm}}$ ± 3% from a Magboltz calculation.

5.6. Deformations in the pixel plane

It is important to measure possible deformations in the pixel plane (xy), because for applications in a TPC this affects the momentum resolution. Because of limited statistics, the mean transverse (x) residuals are calculated in bins of 4 × 4 pixels over the quad plane using the tracks defined by the telescope, see Fig. 8. Only bins with more than 800 entries are shown.

A distortion is present near the edges of the chips. The cause is twofold; firstly there is a geometrical bias at the edge of the detector because only part of the ionization cloud can be detected. Secondly, the grounded region at the edge of the Timepix3 die causes a non-uniformity of the electric field.

An empirically selected function of four Cauchy (Breit–Wigner) functions can be fitted to the geometrical bias and the non-uniformity of the field. Near the top and bottom edges the size of the deformations is different, as such – while keeping the other parameters fixed – a 4th

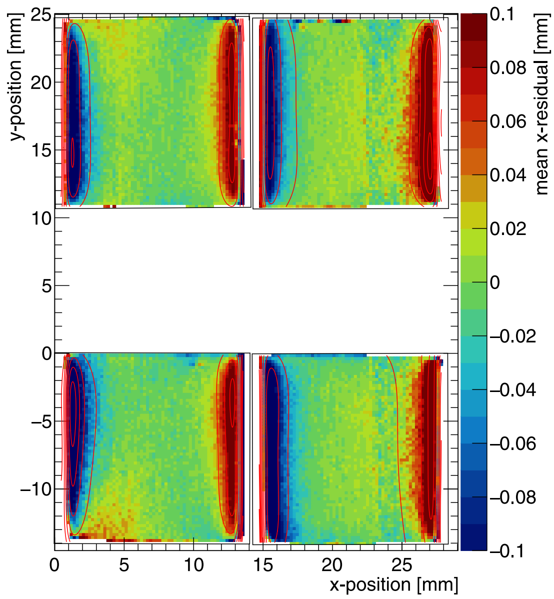

Fig. 8. Mean residuals in the pixel plane (x-residuals) at the expected hit position, fitted with Eq. (4) (red contours).

order polynomial function in y was fitted in a second step to set the scale. All in all, the fitted function is given by:

$$\delta x_{\text{deformations}} = \sum_{j=0}^{4} \left(\frac{1}{\pi} \frac{\gamma_j}{(x - d_j)^2 + \gamma_j^2} \sum_{i=0}^{4} \left(c_{ij} y^i \right) \right), \tag{4}$$

where d_j and γ_j are the location and scale parameters of the Cauchy distributions. c_{ij} are the parameters of the fourth order polynomial.

The outlines of the fitted function are shown in Fig. 8. The fitted function can be used as a correction by subtracting it from the mean residuals. The result of this procedure is shown in Fig. 9.

The r.m.s. of the distribution of the measured mean residual over the surface – or the systematic error for a measurement before the correction in the quad plane – is 31 μm. After subtraction of the fitted correction function (4), the r.m.s. of the mean values is 13 μm over the whole plane and 9 μm in the selected region 2 mm from the edges indicated by a black outline. The distribution of the mean x-residuals after correction are shown in Fig. 10. The distortions could be further reduced by improving the homogeneity of the electric field near the dyke e.g. by adding a field wire above the quad detector at the boundaries between the neighboring chips.

5.7. Deformations in the drift direction

A similar measurement is done for distortions in the drift direction. In Fig. 11 the mean longitudinal (z) residuals are shown in bins of 4×4 pixels over the quad plane using the tracks defined by the telescope. Only bins with more than 800 entries are shown. As shown in Fig. 10, the r.m.s. of the distortion is 19 μm (0.35 ns) and 14 μm (0.26 ns) in the black outlined central area 2 mm from the edges.

5.8. Quad detector resolution

The overall accuracy of a track position measurement using the quad detector can be tested by comparing the quad track to the telescope track. The difference will be a combination of statistical errors, systematic errors and multiple scattering contributions. Here it is important to estimate the systematical error, because multiple scattering occurs primarily outside the fiducial gas volume, and in applications with multiple quad modules the statistical errors will be further reduced.

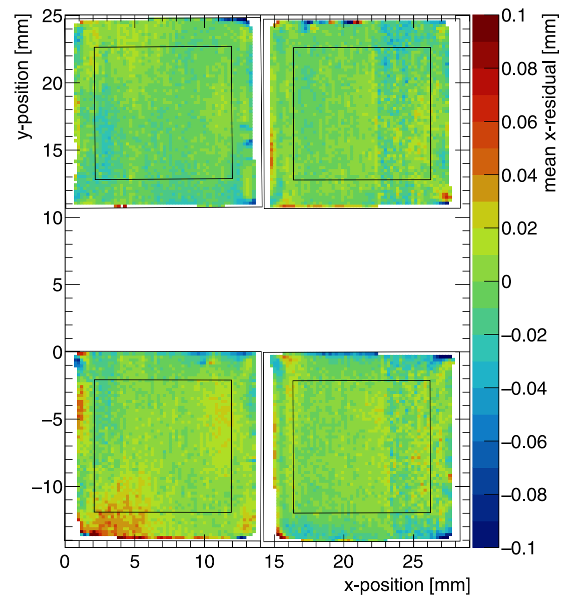

Fig. 9. Mean residuals in the pixel plane (x-residuals) at the expected hit position after subtracting the fitted edge deformations using Eq. (4).

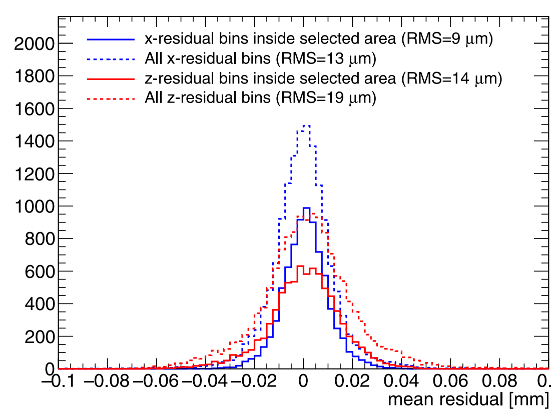

Fig. 10. Distribution of the mean residuals from 4×4 bins in Fig. 9 (x-residuals) and Fig. 11 (z-residuals).

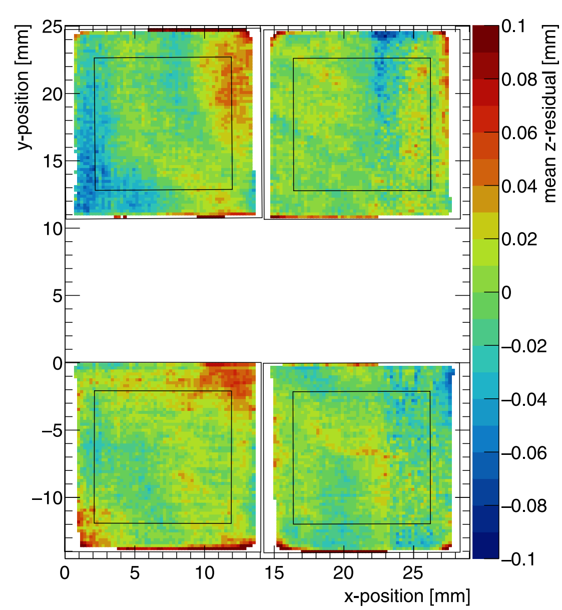

Fig. 11. Mean residuals in the drift direction (z-residuals) at the expected hit position.

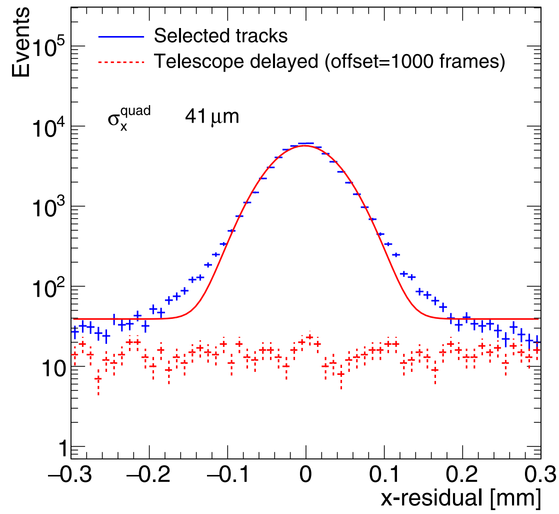

Fig. 12. Difference between mean hit position and track prediction in the pixel plane, fitted with a Gaussian plus a flat background (solid red line). In comparison the background tracks are shown (dashed red), acquired by offsetting the telescope by 1000 frames.

Fig. 12 displays the difference between the mean position of all quad track hits and the telescope track in the fiducial region. The distribution has long tails, which are in part from unrelated background tracks that are erroneously matched. The number of background tracks is estimated by shifting the telescope timing by 1000 frames and is shown for comparison. In the fit, these tracks are accounted for by introducing a constant offset.

A fit with a Gaussian function with constant offset yields a standard deviation σ_x^{quad} of 41 µm. This value is the result of various contributions. Firstly, the statistical precision of a position measurement is acquired from a track fit of the quad hits with hit errors. This statistical precision of the position at the center of the quad is 25 µm. Furthermore, there is a systematic deviation of 9 µm in the pixel plane in the fiducial region after the correction as discussed in Section 5.6. Additionally, there is a systematic deviation in the x-direction of 17 µm along the drift direction most likely due to electric field inhomogeneities. This is the x-deviation as a function of z-position. which should not be confused with the z-deviation as a function of x and y-position that was mentioned before in Section 5.7.

In addition, the precision is limited due to multiple scattering in the setup. The precision was calculated with a simple simulation of the setup using the approach to multiple scattering suggested by reference [12]. The setup has multiple scattering contributions from the telescope planes (0.075% X_0 per plane) [8], the air (0.084% X_0), the TPC gas (0.09% X_0) and the two Kapton foils (0.035% X_0) [12]. By comparing the track angle in the first three telescope planes and the second three telescope planes, the total radiation length of the setup is estimated to be 0.82% X_0 (0.66% X_0 expected). From the simulation the multiple scattering contribution at the position of the quad center is estimated to be 22 µm.

An overview of the contributing errors is given in Table 3. In the end, there is still a small unidentified systematic error of 14 µm.

6. Conclusion and outlook

A quad module with four Timepix3 based GridPixes has been designed and realized. The module has dimensions of 39.6 mm × 28.38 mm and an active surface of 68.9%. The quad module was embedded in a TPC detector and operated at the ELSA test beam facility. The single electron resolutions in the transverse and longitudinal planes are similar to the results obtained for the single-chip detector [5] and primarily limited by diffusion. It is shown that a systematic error from the quad detector for the distortions over the pixel plane of 13 µm (9 µm in the central region) has been achieved. The demonstrated resolution of the setup is 41 µm, of which the statistical error is 25 µm, the error caused by multiple scattering in the setup is 22 µm and the total systematic error is 24 µm.

The next step is to demonstrate a large detection area with the quad module as a building block and confirm the potential of the GridPix technology for large detectors. A new detector with 8 quad modules carrying a total of 32 Timepix3 Gridpix chips is under construction.

Table 3
Overview of the errors on the difference between mean hit position and track prediction in the pixel plane.

Observed standard deviation σ_x^{quad}	41 µm
Statistical quad detector error	25 µm
Statistical telescope error	2 µm
Systematics over the pixel plane (corrected)	9 µm
Systematics along the drift direction	17 µm
Multiple scattering contribution	22 µm
Remaining systematic error	14 µm

Declaration of competing interest

The authors declare that they have no known competing financial interests or personal relationships that could have appeared to influence the work reported in this paper.

CRediT authorship contribution statement

C. Ligtenberg: Investigation, Formal analysis, Writing - original draft. **Y. Bilevych:** Investigation. **K. Desch:** Investigation. **H. van der Graaf:** Investigation. **M. Gruber:** Investigation. **F. Hartjes:** Investigation. **K. Heijhoff:** Investigation. **J. Kaminski:** Investigation. **P.M. Kluit:** Investigation. **N. van der Kolk:** Investigation. **G. Raven:** Investigation. **T. Schiffer:** Investigation. **J. Timmermans:** Investigation.

Acknowledgments

This research was funded by the Netherlands Organisation for Scientific Research NWO. The authors want to thank the support of the mechanical and electronics departments at Nikhef and the accelerator group at the ELSA facility in Bonn. Their gratitude is extended to the Bonn SiLab group for providing the beam telescope.

References

[1] P. Colas, A.P. Colijn, A. Fornaini, Y. Giomataris, H. van der Graaf, E.H.M. Heijne, X. Llopart, J. Schmitz, J. Timmermans, J.L. Visschers, The readout of a GEM- or micromegas-equipped TPC by means of the Medipix2 CMOS sensor as direct anode, Nucl. Instrum. Methods A535 (2004) 506–510, http://dx.doi.org/10.1016/j.nima.2004.07.180.

[2] M. Campbell, M. Chefdeville, P. Colas, A.P. Colijn, A. Fornaini, I. Giomataris, H. van der Graaf, E.H.M. Heijne, P. Kluit, X. Llopart-Cudie, J. Schmitz, J. Timmermans, J.L. Visschers, Detection of single electrons by means of a micromegas-covered MediPix2 pixel CMOS readout circuit, Nucl. Instrum. Methods A540 (2005) 295–304, http://dx.doi.org/10.1016/j.nima.2004.11.036, arXiv:physics/0409048.

[3] J. Kaminski, Y. Bilevych, K. Desch, C. Krieger, M. Lupberger, GridPix detectors - introduction and applications, Nucl. Instrum. Methods A845 (2017) 233–235, http://dx.doi.org/10.1016/j.nima.2016.05.134.

[4] T. Poikela, J. Plosila, T. Westerlund, M. Campbell, M. De Gaspari, X. Llopart, V. Gromov, R. Kluit, M. van Beuzekom, F. Zappon, V. Zivkovic, C. Brezina, K. Desch, Y. Fu, A. Kruth, Timepix3: a 65K channel hybrid pixel readout chip with simultaneous ToA/ToT and sparse readout, J. Instrum. 9 (05) (2014) C05013, URL http://stacks.iop.org/1748-0221/9/i=05/a=C05013.

[5] C. Ligtenberg, K. Heijhoff, Y. Bilevych, K. Desch, H. van der Graaf, F. Hartjes, J. Kaminski, P.M. Kluit, G. Raven, T. Schiffer, J. Timmermans, Performance of a GridPix detector based on the Timepix3 chip, Nucl. Instrum. Methods A908 (2018) 18–23, http://dx.doi.org/10.1016/j.nima.2018.08.012.

[6] C. Krieger, J. Kaminski, M. Lupberger, K. Desch, A GridPix-based X-ray detector for the CAST experiment, Nucl. Instrum. Methods A867 (2017) 101–107, http://dx.doi.org/10.1016/j.nima.2017.04.007.

[7] J. Visser, M. van Beuzekom, H. Boterenbrood, B. van der Heijden, J.I. Muñoz, S. Kulis, B. Munneke, F. Schreuder, SPIDR: a read-out system for Medipix3 & Timepix3, J. Instrum. 10 (12) (2015) C12028, http://dx.doi.org/10.1088/1748-0221/10/12/C12028.

[8] H. Jansen, S. Spannagel, J. Behr, A. Bulgheroni, G. Claus, E. Corrin, D. Cussans, J. Dreyling-Eschweiler, D. Eckstein, T. Eichhorn, M. Goffe, I.M. Gregor, D. Haas, C. Muhl, H. Perrey, R. Peschke, P. Roloff, I. Rubinskiy, M. Winter, Performance of the EUDET-type beam telescopes, EPJ Tech. Instrum. 3 (1) (2016) 7, http://dx.doi.org/10.1140/epjti/s40485-016-0033-2.

[9] D. Cussans, Description of the JRA1 Trigger Logic Unit (TLU), v0.2c, EUDET Collaboration, 2009, URL https://www.eudet.org/e26/e28/e42441/e57298/EUDET-MEMO-2009-04.pdf.

[10] R. Veenhof, Garfield - simulation of gaseous detectors, Version 9, Reference W5050, 1984-2010, URL https://garfield.web.cern.ch.

[11] S.F. Biagi, Monte Carlo simulation of electron drift and diffusion in counting gases under the influence of electric and magnetic fields, Nucl. Instrum. Methods A421 (1–2) (1999) 234–240, http://dx.doi.org/10.1016/S0168-9002(98)01233-9, URL https://magboltz.web.cern.ch/magboltz/.

[12] C. Patrignani, et al., Particle Data Group, Review of particle physics, Chin. J. Phys C40 (10) (2016) 100001, http://dx.doi.org/10.1088/1674-1137/40/10/100001, Section 33.3.